Article ID: WMC005076 ISSN 2046-1690

The Zika Virus sfRNA Secondary Structure Reveals a miR-147a Homologue that Targets Neurofascin as a Potential Cause of its Neurologic Syndromes

Peer review status:
No

Corresponding Author:
Dr. Robert Ricketson,
Senior Research Scientist, Institute of Pure and Applied Knowledge, 528 NW 173rd Street, 73012 - United States of America

Submitting Author:
Dr. Robert Ricketson,
Senior Research Scientist, Institute of Pure and Applied Knowledge, 528 NW 173rd Street, 73012 - United States of America

Other Authors:
Dr. James Lyons-Weiler,
President and CEO, Institute of Pure and Applied Knowledge, 2912 Kilcairn Lane\nAllison Park, PA \n, 15101 - United States of America

Article ID: WMC005076

Article Type: Research articles

Submitted on:24-Mar-2016, 06:48:31 AM GMT **Published on:** 24-Mar-2016, 01:36:35 PM GMT

Article URL: http://www.webmedcentral.com/article_view/5076

Subject Categories:VIROLOGY

Keywords: Zika virus, Zika virus miRNA, Zika virus disease, Microcephaly, Guillan-Barre Syndrome, Zika virus neurotropism

How to cite the article: Ricketson R, Lyons-Weiler J. The Zika Virus sfRNA Secondary Structure Reveals a miR-147a Homologue that Targets Neurofascin as a Potential Cause of its Neurologic Syndromes. WebmedCentral VIROLOGY 2016;7(3):WMC005076

Source(s) of Funding:

Funding was provided by the Institute of Pure and Applied Knowledge.

Competing Interests:

No competing interests

Additional Files:

The Zika Virus sfRNA Secondary Structure Reveals a miR-147a Homologue that Targets Neurofascin as a Potential Cause of its Neurologic Syndromes

Author(s): Ricketson R, Lyons-Weiler J

Abstract

Pathologies associated with Zika virus infection include partial progressive paralysis (Guillan Barre Syndrome) and microcephaly in Brazil and Panama. We identified an 85 nucleotide stem loop structure in the 3' end of Zika virus sfRNA (position (343-428) with the canonical structural and sequence characteristics of a miRNA. In comparison, the West Nile Virus has been previously demonstrated to contain a miRNA in its 3' untranslated (UTR) sfRNA region. The West Nile Virus miRNA, KUN-mir-1, was found to be 81 nucleotides in length (492-573) and 58% conserved overall as to the corresponding Zika virus stem loop nucleotide sequence. The majority on the sequence homology was in the terminal loop (78%). The 40 nucleotide (nt) 3p arm demonstrated 60% homology, decreasing at the distal segment. The 5p arm demonstrates on 42% sequence homology.

The Zika virus stem loop in this study was identified to contain a hairpin structure in the 3' end of the Zika virus sfRNA 3' UTR segment predicted to contain a miRNA with significant homology to human hsa-mir-147a. Target analysis identified 241 human transcripts which include, but not limited to, neurofascin, synaptic vesicle glycoprotein 2A, neurofibromin 1, SAM and SH3 domain containing 1, neurogenin 2, in addition to multiple immune transcripts.

Autoantibodies to neurofascin have been reported in in Guillan-Barre Syndrome (GBS), but have not yet been reported in or after Zika virus infection. A significant 9 mer match exists between the Zika virus miRNA 3p arm and the Neurofascin 3'UTR seed region, CCACACA. In contrast to West Nile Virus, GATA4 was not predicted to be, nor was identified in the MirBaseDB, to be a target of the Zika virus miRNA.

These computational results indicate highly plausible mechanisms explaining the neurologic syndromes such a Guillan-Barre Syndrome and microcephaly associated with Zika virus infection, and warrant further investigation.

Introduction

Between January 2007 and February 2016, a total of 41 countries and territories reported local transmission of Zika virus; this includes 36 countries which reported local transmission between 2015 and 2016. Six countries (Brazil, French Polynesia, El Salvador, Venezuela, Colombia and Suriname) have reported an increase in the incidence of cases of microcephaly and/or Guillain-Barré syndrome (GBS) following a Zika virus outbreak. Puerto Rico and Martinique have also reported cases of GBS associated with Zika virus infection, but without evidence of an overall increase in the incidence of GBS. A number of concurrent events have occurred in Brazil, each of which provides an alternative hypothesis for microcephaly and Guillan-Barre Syndrome worth consideration.

We previously reported on several hypotheses as to the pathogenesis in Zika virus neurologic associations in this outbreak. Here, we further append the discussion towards the identification of a potential virus encoded miRNA in the subgenomic Flavivirus (sfRNA) 3' UTR in Zika virus. We identified specific plausible mechanisms for microencephaly, including:

1. Direct Zika-related microcephaly through unspecified mechanisms;

2. Molecular mimicry of Bordetella pertussis peptides in tetanus-diphtheria-acellular pertussis (TdaP)

Vaccine and whole-cell Bordetella pertussis vaccine (wP);

3. Pestivus virus contamination in locally produced whole-cell Bordetella pertussis vaccine;

4. Glyphosate toxicity in bovine products in TdaP or wP vaccine (via interactions w/aluminum in the vaccine;

5. Zika p53-BAX induced apoptosis, as in Rubella virus;

6. Use of paracetamol (Acetaminophen) to reduce fever in pregnancy and in newborns;

7. Horizontal transfer of piggyBAC transposon from released GMO mosquitos;

8. Interactions among any of the above.

Importantly, microcephaly has not yet been reported due to Zika infection outside of Brazil, except one report of one case in Panama. There have been thousands of pregnancies outside of Brazil with Zika virus infection but no sign of microcephaly.

The Zika virus belongs to the genus Flavivirus, and is related to the Dengue, Yellow Fever, Japanese encephalitis, Chikungunya, and West Nile viruses. Like other Flaviviruses, Zika virus (ZIKV) contains a nonsegmented, single-stranded, positive-sense, single-stranded RNA genome. The open reading frame of the Zika virus reads as follows: 5′ UTR-Capsid [C], prM-E-NS1-NS2A-NS2B-NS3-NS4A-NS4B-NS5 (RNA-dependent RNA polymerase)-3′ UTR. The polyprotein is subsequently cleaved into capsid (C), precursor membrane (prM), envelope (E), and non-structural proteins. The structural proteins encapsulate the viral genome. The replicated RNA strand is held within a nucleocapsid formed from 12-kDa protein blocks; the capsid is contained within a host-derived membrane modified with two viral glycoproteins.

Prior studies have demonstrated that the highly conserved secondary structures within the subgenomic Flavivirus RNA (sfRNA) in the West Nile Virus 3' UTR were resistant to host nucleases and responsible for the observed cytopathology and pathogenicity. It was subsequently demonstrated that the 3' end of the West Nile Virus sfRNA encoded a miRNA, KUN-miR-1, processed in the cytoplasm via Dicer-1 which increased viral RNA replication by inducing GATA4. As both West Nile Virus and Zika virus share similar sequences homology in the region of the sfRNA, we investigated the possibility that the Zika virus could similarly encode a miRNA with different human targets leading to a potential cause of the neurologic syndromes reported in Zika virus infection.

Here, as part of our attempts to exhaust possible causal hypotheses of Zika virus pathogenesis, we explore the possibility that Zika virus encodes one or more miRNA's in the subgenomic Flavivirus (sfRNA) 3' UTR in Zika virus involved in Guillan-Barre Syndrome.

The Zika virus belongs to Flaviviridae and the genus Flavivirus, and is related to the Dengue, Yellow fever, Japanese encephalitis, Chikungunya, and West Nile viruses. Like other flaviviruses, Zika virus is enveloped and has a nonsegmented, single-stranded, positive-sense, single-stranded RNA genome. The open reading frame of the Zika virus reads as follows: 5′ UTR-Capsid [C], prM-E-NS1-NS2A-NS2B-NS3-NS4A-NS4B-N?S5 (RNA-dependent RNA polymerase)-3′ UTR. The polyprotein is subsequently cleaved into capsid (C), precursor membrane (prM), envelope (E), and non-structural proteins. The structural proteins encapsulate the viral genome. The replicated RNA strand is held within a nucleocapsid formed from 12-kDa protein blocks; the capsid is contained within a host-derived membrane modified with two viral glycoproteins [1].

Pijman et al in 2008 [2] demonstrated that the highly conserved secondary structures within the subgenomic Flavivirus RNA (sfRNA) of the 3' UTR were resistant to host nucleases and responsible for the observed cytopathology and pathogenicity. Furthermore, the sfRNA of Flaviviruses accumulated in the brain, was not packaged into virions, and was not a product of RNA self-cleavage. The sfRNA was readily detected in both replicating and *nonreplicating* transfected cells. This appeared to demonstrate that neither viral RNA replication, viral proteins, nor the 5' UTR were essential for sfRNA generation. The full length sfRNA was shown to produce cytopathology in cell culture but cell death (apoptosis) only occurred in the presence of viral infection, alluding to addition factors such as p53-BAX/Caspace pathways we have recently reported 37].

Hussain et al in 2012 [36] identified a viral-encoded miRNA within the sfRNA segment of West Nile Virus, KUN-miR-1, in the 3' end of the sfRNA. Levels of KUN-miR-1 were significantly reduced after silencing Dicer-1 and replication of the virus was reduced upon inhibition of KUN-miR-1. KUN-miR-1 was subsequently found to increased accumulation of GATA4 mRNA and virus RNA replication. The WNV miRNA was identified to be produced by cytoplasmic pathway, thereby utilizing only Dicer and independent of the nuclear endonuclease Drosha.–

As both West Nile Virus and Zika virus share similar sequence and secondary structural homology in the region of the sfRNA, we investigated the possibility that the Zika virus could similarly encode a miRNA with different human targets leading to a potential cause of the neurologic syndromes reported in Zika virus infection.

MicroRNAs (miRNAs) are small. ~22 nt in length RNAs that are involved in regulation of gene expression. MiRNAs silence gene expression by directing repressive protein complexes to the 3′ untranslated region (UTR) of target messenger RNA (mRNA) transcripts. The first miRNAs were discovered in *Caenorhabditis elegans* [19] and have been

extensively identified to represent a large family of evolutionarily conserved genes among insects, nematodes, and humans [3-5]

In host–pathogen interactions, miRNAs play a role in regulating the innate immune response, adaptive immune cell differentiation, metabolism, apoptosis, cell proliferation, cancer, and maintenance of homeostasis during stress. Canonical miRNAs derive from longer precursor *primary* transcripts (pri-miRNAs. *Pri*-miRNAs contain at least one, but often several, precursor(s) of imperfectly complementary stem-loop hairpin structures.

Precursor miRNAs (*pre-miRNAs*) are generated from the larger 32-35 base pair pri-miRNA via the endonuclease Drosha with 3' overhangs of 2 nucleotides [5]. Drosha, along with DGCR8, combine to form the microprocessor complex (6-8). The Drosha-DGCR8 microprocessor complex binds to the pri-miRNA, at the base of the hairpin stem, typically a 5' UG/AG motif and a CNNC motif at the 3' end. Fang et al reported in 2015 that the basal UG and apical UGU motifs at the junctions of single-stranded and double-stranded RNA regions of the pri-miRNA that the Drosha-FDGR8 Microprocessor complex recognizes either or both of these junctions [9, 10]. Biochemical analyses have shown that Drosha recognizes the basal junction and the DGCR8 dimer recognizes the apical junction [11, 12]. Their analysis further determined the following requirements:

1. A mismatched GUG motif in the basal stem region
2. A preference for maintaining or improving base pairing throughout the remainder of the stem
3. A stem length preference of ~35 base pairs
4. A basal U(A)G motif
5. An apical U(A)G motif in the terminal loop

FIGURE 1. Features of a Canonical miRNA

The 5' flanking sequence contains a UG motif whereby the uracil is occasionally substituted by an adenine (A) with continued processing towards a mature miRNA. A GUG mismatch motif is located in the proximal stem loop structure duplex, and an apical (G)UG motif is identified in the 5p-terminal loop junction. The 3p arm usually terminates in a CNNC motif (not shown).

The newly liberated ~60-80 nucleotide hairpin pre-miRNA is then exported from the nucleus to the cytoplasm via the RAN-GTPase Exportin 5. In the cytoplasm, the pre-miRNAs are cleaved by the endonuclease Dicer.

Dicer-mediated cleavage produces a transient ~22 nt duplex RNA, of which one strand ("guide" strand) is incorporated into the RNA-induced silencing complex (RISC). The "passenger" strand is less likely to associate with RISC. RISC is a multiprotein complex including the Argonaute (Ago) protein. Ago-loaded miRNAs (miRISC) typically bind to target transcripts and inhibit gene expression.

Recently, diverse DNA virus families, and some + RNA genomes, have been found to encode miRNAs **(TABLE 1].** – strand RNA viruses have been less likely to form miRNA but have recently been reported in the Zaire ebolavirus [13].

Within the group of reported viral encoded miRNAs, two distinct groups exist. Some viral miRNAs mimic host miRNAs and take advantage of conserved networks of host miRNA target sites while other viral miRNAs do not share common target sites conserved for host miRNAs. RNA viruses represent a challenge in that their replication occurs in the cytoplasm, and thereby bypassing the initial nuclear Drosha cleavage. In that regard, noncanonical miRNA biogenesis pathways have been identified [14].

Table 1. Viral-Encoded miRNAs Identified in miRBase

Bovine foamy virus	2 precursors, 4 mature
Bovine herpesvirus 1	10 precursors , 12 mature
Bovine herpesvirus 5	5 precursors, 5 mature
BK polyomavirus	1 precursor, 2 mature
Bovine leukemia virus	5 precursors, 10 mature [K02120.1]
Bandicoot papillomatosis carcinomatosis virus type 1	1 precursor, 1 mature
Bandicoot papillomatosis carcinomatosis virus type 2	1 precursor, 1 mature
Duck enteritis virus	24 precursors, 33 mature
Epstein Barr virus	25 precursors, 44 mature [EMBL:AJ507799.2]
Herpes B virus	12 precursors, 15 mature [Refseq:NC_004812]
Human cytomegalovirus	15 precursors, 26 mature [EMBL:X17403.1]
Human herpesvirus 6B	4 precursors, 8 mature
Human immunodeficiency virus 1	3 precursors, 4 mature
Herpes Simplex Virus 1	18 precursors, 27 mature
Herpes Simplex Virus 2	18 precursors, 24 mature
Herpesvirus saimiri strain A11	3 precursors, 6 mature
Herpesvirus of turkeys	17 precursors, 28 mature
Infectious laryngotracheitis virus	7 precursors, 10 mature
JC polyomavirus (1 precursor	2 mature
Kaposi sarcoma-associated herpesvirus	13 precursors, 25 mature [EMBL:U75698.1]
Mouse cytomegalovirus	18 precursors, 29 mature
Merkel cell polyomavirus	1 precursor, 2 mature
Mareks disease virus type 1	14 precursors, 26 mature [EMBL:AF243438.1]
Mareks disease virus type 2	18 precursors, 36 mature
Mouse gammaherpesvirus 68	15 precursors, 28 mature [EMBL:U97553.1]
Pseudorabies virus	13 precursors, 13 mature
Rhesus lymphocryptovirus	36 precursors, 68 mature
Rhesus monkey rhadinovirus	7 precursors, 11 mature [EMBL:AF210726.1]
Simian virus 40	1 precursor, 2 mature

The majority of host and viral miRNAs are processed through the canonical pathway. Other viruses utilize noncanonical mechanisms in the biogenesis of pre-miRNA molecules and may not demonstrate the classic structural properties. For example, the validated Epstein-Bar miRNA, ebv-miR-BART1-5p MIMAT0000999, as shown below contain 26 bp, and an apical loop of only 6 nt, without an apical GUG **(FIGURE 2)**.

Figure 2. Secondary structure of ebv-mir-BART1

The secondary structure of the validated Epstein - Barr virus miRNA, ebv-mir-BART1, was generated with Mfold [15]. The 5' terminus contains a UG motif and a UGU mismatch region. The Terminal loop is 6 nt in length,, and the GUG motif is not predicted to be in the 5' region of the terminal loop

but in the downstream region of the 5' arm. The 3' arm terminates in a CCCG sequence, in contrast to the canonical CNNC motif. Despite these deviations from the canonical sequence-structure definitions of a novel miRNA, the ebv-mir-BART1 miRNA is a valid Epstein-Barr virus encoded miRNA.

The World Health Organization (WHO) recently determined 5 priority research areas for the Zika virus outbreak to be:

1. Causality Framework
2. Sexual Transmission
3. Mosquito Vector Control
4. Natural History of Zika Virus Disease
5. Infection Control

Towards causality of the neurologic deficits, particularly with regards to the incidence of Guillan-Barre Syndrome (GBS), we investigated the possibility of a previously unreported viral-encoded miRNA. As of this report, no definite Flavivirus stem-loop or mature miRNAs have been identified in miRBase. The miRBase database is a searchable database of published miRNA sequences with annotation and target listing. Each entry in the miRBase Sequence database represents a predicted hairpin portion of a miRNA transcript (termed *mir*), with information on the location and sequence of the mature miRNA sequence (termed miR) as well as predicted targets in the 3'UTRs in additional public databases. Both hairpin and mature sequences are available for analysis.

Materials and Methods

Secondary Structure Analysis

The 427 nt 3' UTR of the ZIKV miRNA (gi|226377833:10367-10794) was obtained from the National Center of Biotechnology Information (NCBI) database (5' GCACCAAUUUUAGUGUUGUCAGGCCUGCUAGUCAGCCACAGUUUGGGGAAAG CUGUGCAGCCUGUAACCCCCCCAGGAGAAGCUGGGAAACCAAGCUCAUAGUCAGGCCGAGAACGCCAUGGCACGGAAGAAGCCAUGCUGCCUGUGAGCCCCUCAGAGGACACUGAGUCAAAAAACCCCACGCGCUUGGAAGCGCAGGAUGGGAAAAGAAGGUGGCGACCUUCCCCACCCUUCAAUCUGGGGCCUGAACUGGAGACUAGCUGUGAAUCUCCAGCAGAGGGACUAGUGGUUAGAGGAGACCCCCCGGAAAACGCAAAACAGCAUAUUGACGUGGGAAAGACCAGAGACUCCAUGAGUUUCCACCACGCUGGCCGCCAGGCACAGAUCGCCGAACUUCGGCGGCCGGUGUGGGGAAAUCCAUGGUUUCU-3') and submitted to the Mfold web server [15] with default parameters to identify any potential miRNA stem loop secondary structure as well as the online Vienna webserver. Secondary structures were predicted with RNAFold, formatting the output to base pair probability and positional entropy [16, 17]. Pseudoknots were predicted with RNAstructure, Version 5.8 [18].

Comparison of the secondary structures of the sfRNA 3'UTR of West Nile virus (WNV|gi|11528013:10390-10962), Dengue Virus 1 (DENV1|gb|JQ045634.1|:10252-10699), Chikungunya virus (CHIKV|gb|GU301780.1|:11233-11757), the Japanese encephalitis virus (JEV|gb|AY303791.1|:10395-10970), and Yellow fever virus (YFV|gb|AF094612.1|:10355-10760) was similarly analyzed for potential *pri-miRNA* stem loop sequences and compared with the secondary structure of ZIKV.

MiRNA Stem Loop and Mature miRNA Candidates

Candidate stem loop and mature sequences were then searched in both MiRBase [30-36] and Vir-MiR [19] and filtered to search only for human miRNA homologues (*hsa-miR*) and their human targets. The Vir-MiR Database has 171 accumulated potential miRNA's in Flavivirus with none seen in the closely related Spondweni virus and Dengue virus group (**Table 2**). Zika virus is not listed under any taxonomy group. West Nile Virus (GenBank 11528013) is listed in the Japanese encephalitis group with six potential candidates. Three are located in the 3' untranslated region (10367-10794). The other candidates are identified within the coding sequence and not identified to be within the 5' UTR (1-106) were excluded from consideration (**Table 3**).

Table 2. Flavivirus miRNA Vir-miR database

Flavivirus (171)	
Dengue virus group	0
Japanese encephalitis virus group	37
Kokobera virus group	0
Modoc virus group	5
mosquito-borne viruses	0
Ntaya virus group	5
Rio Bravo virus group	7
Seaborne tick-borne virus group	0
Spondweni virus group	0
tick-borne encephalitis virus group	89
unclassified Flavivirus	18
Yaounde virus	0
Yellow fever virus group	10

Table 3. West Nile Virus Potential miRNA segment-Vir-MiR database 2016

ID-	strand	start	length	sRNA loop score	core MFE.	NP ORF	Known viral miRNA
3377	+	189	89	24.5	-26.1	NP_041724	None
3378	+	7267	90	20.5	-32.8	NP_041724	None
3379	+	10884	79	22	-29.6	None	None
3380	-	8371	89	21	-25.3	NP_041724	None
3381	-	10604	89	23	-24.9	None	None
3382	-	10961	77	22.5	-32.5	None	None

Multiple Sequence Analysis

The full length sfRNA 3' UTR nucleotide sequences

from Zika virus (ZIKV (gi|226377833:10367-10794), West Nile virus (WNV|gi|11528013:10390-10962), Dengue Virus 1 (DENV1|gb|JQ045634.1|:10252-10699), Chikungunya virus (CHIKV|gb|GU301780.1|:11233-11757), the Japanese encephalitis virus (JEV|gb|AY303791.1|:10395-10970), and Yellow fever virus (YFV|gb|AF094612.1|:10355-10760) were then analyzed using Clustal Omega within Jalview 2.9.0b2 using default parameters [20].

Hybridization

Potential miRNA-target hybrids were analyzed using the RNAHybrid webserver Bielefeld Bioinformatics Server [21, 22]. RNAHybrid predicts multiple potential binding sites of miRNAs in large target RNAs by finding the energetically most favorable hybridization sites of a small RNA in a large RNA sequences.

Results

Secondary Structure of the ZIKV sfRNA

Mfold revealed a stem loop structure with significant positional entropy of ~87 base pairs from position 341-428 in the terminal 3' region of the ZIKV sfRNA (FIGURE 3). The 5p arm contains an AG motif as well as a UG motif in the 5' overhang that could be recognized by Drosha to cleave the stem loop. There does appear to be a GUG mismatch motif in the proximal 5' region in the stem loop. The 3p arm terminates in a stable paired construct without overhang. The terminal loop is a variable 9 nt in length and does not appear to contain the GUG motif (FIGURE 4). However, as mentioned earlier, this may impair efficient recognition and processing, other known viral-encoded miRNAs also do not contain that motif suggesting the GUG motif is not a requisite for processing to a pre-miRNA.

Figure 3. Secondary Structure of the ZIKV 3' UTR sfRNA

The secondary structure of the Zika virus sfRNA of the 3' UTR (428 nt) was generated in Mfold using default parameters. The stem loop structure (MFE -167.68) from 343-428 is highlighted. Pseudoknots cannot be predicted in Mfold and predictions of peudoknots were obtained with RNAStructure and visualized with VARNA [23].

Figure 4. ZIKV Predicted Stem Loop Structure

The 5' end on the predicted stem loop (343-428) contains a basal AG motif similar to the West Nile Virus miRNA, a GUG mismatch in the downstream 5p arm, a 9 nucleotide terminal loop with an apical AG motif similar to the West Nile Virus miRNA, but does not have a 3p CNNC motif. All flavivirus sfRNAs terminate at the 3' end without a CNNC motif and the West Nile Virus miRNA has been demonsrated to bypass the endonucease Drosha and be processed in the cytoplasm.-

Pseudoknots cannot be predicted in Mfold. A circular structure diagram of the partition function to predict potential pseudoknots was obtained using RNAStructure, version 5.8 (Figure 5) and the secondary structure was generated with VARNA version 3.93 [23] (FIGURE 6). 5 regions of pseudoknot formation were predicted ({1-3->26-28}; {31-32->67-68}, {91-92->159-160}; 107-110->196-200}; {237-243->302-308}) from position 1-308. No pseudoknot was predicted to lay within the stable stem loop located within the the 3' region of the ZIKV sfRNA.

Figure 5. Circular plot of potential pseuknots in ZIKV sfRNA (RNAStructure)

A partition function, maximum free energy (MFE) structure, and pseudoknot prediction was performed using RNAStructure. The resultant sequence-structure was submitted to RNAFold for secondary structure visualization for calculation of positional entropy. All predicted pseudoknots were upstream from the stable, conserned stem loop structure in the 3' region 383-428 in the Zika virs sfRNA.

Figure 6. Pseudoknot Secondary Structure Prediction of ZIKV (Natal, 2016)

A pseudoknot dot-plot structure was generated in RNAStructure and RNAFold. 5 regions of pseudoknot formation were predicted ({1-3->26-28}; {31-32->67-68}, {91-92->159-160}; 107-110->196-200}; {237-243->302-308}) from position 1-308 in the Zika virus sfRNA. The 3' stem loop was downstream and was not involved in a predicted pseudoknot conformation. The secondary structure was visualized utilizing Pseudoviewer 2.5 (Panel A) [46-49] and the Visualization Applet for RNA (VARNA-Panel B) [23].

SECONDARY STRUCTURE COMPARISON OF THE sfRNA IN FLAVIVIRUS

Base pair probability secondary structures were obtained and visualized with RNAFold. A conserved secondary stem loop within the 3' region was observed in ZIKV, WNV, JEV, and YFV (Figure 7). ZIKV demonstrated the best base pair probability and positional entropy within the predicted stem loop as compared to WNV, JEV, and YFV. The long stem loop was not observed in either CHIKV or DENV1.

FIGURE 7. Comparative Secondary Structures in Flavivirus

Secondary structures of the sfRNA from ZIKV, WNV, DENV1, CHIKV, Japanese encephalitis virus, and Yellow Fever Virus were generated with RNAFold, formatted for base pair probability and positional entropy. A highly conserved 3' stem loop was identified between ZIKV (383-428), WNV (492-573), Japanese encephalitis virus (497-576), and Yellow Fever Virus (318-406). The 3' region was significantly truncated in both DENV1 and CHIKV with respect the ZIKV sfRNA sequence.

MULTIPLE SEQUENCE ALIGNMENT IN FLAVIVIRUS

A global MSA of representative sequences from Zika virus (ZIKV (gi|226377833:10367-10794), West Nile virus (WNV|gi|11528013:10390-10962), Dengue Virus 1 (DENV1|gb|JQ045634.1|:10252-10699), Chikungunya virus (CHIKV|gb|GU301780.1|:11233-11757), the Japanese encephalitis virus (JEV|gb|AY303791.1|:10395-10970), and Yellow fever virus (YFV|gb|AF094612.1|:10355-10760) were then analyzed using Clustal Omega within Jalview, version 2.9. The coloring was set to percent identity for region of conservation. The length of the sfRNA ranged from 406 nt (5' truncated in YFV) to 576 nt (JEV). The regions of conservation were identified at positions 15-27, 56-78. 137-146, 213-222, 242-265, 277-302, 316-341, and 378-390. (Figure 8)

Within the stem loop of ZIKV, the 3' region and the terminal loop demonstrated the greatest overall conservation as compared to ZIKV (FIGURE 9). CHIKV was poorly conserved as to ZIKV overall. JEV and DENV1 were both truncated at the 3' arm which would affect base pairing in a miRNA model as suggested by the comparative secondary structures. The West Nile Virus sequence-structure homology was strongest sequence homology was in the terminal loop (78%). The 40 nt 3p arm demonstrated 60% sequence homology, decreasing at the distal segment. The 5p arm demonstrates only 42% sequence homology (Figures 8 and 9). This would suggest that any potential viral-encoded mature miRNA generated by ZIKV would be unique to the species.

FIGURE 8. MSA sfRNA with Zika virus, West Nile Virus, Dengue virus 1 (DENV1), Dengue virus 2 (DENV2), Cikungunya virus (CHIKV), Japanese encephalitis virus, and Yellow fever virus

The length of the sfRNA ranged from 406 (Yellow Fever Virus)-573 (West Nile Virus0. With respect to the sfRNA of ZIKV, the overall percent identity with West Nile Virus was 54.88%, DENV1 63.98%, CHIKV 46.55%, Japanese encephalitis virus 54.34%, and Yellow fever virus 55.69%. The 3' region from position 208-423 of ZIKV demonstrated the greatest homology. The Dengue virus sfRNA and Chikungunya sfRNA were 3' truncated with respect to the Zika virus stem loop, West Nile Virus, Japanese encephalitis virus, and Yellow Fever Virus sfRNA sequences.

FIGURE 9. MSA ZIKV Stem_Loop with West Nile Virus, Dengue virus 1 (DENV1), Dengue virus 2 (DENV2), Chikungunya virus (CHIKV), Japanese encephalitis virus, and Yellow fever virus

Computational studies identified an 84 nucleotide stem loop structure in the 3' end of Zika virus sfRNA (position (343-428), 6 nucleotides (nt) downstream from the Zika virus sfRNA 5' flanking sequence, UGGAA. DENV2, DENV1, and CHIKV sfRNA sequences were truncated at the 3' region with respect to ZIKV.

The West Nile virus stem loop was 81 nucleotides in length (492-573), and 58% conserved overall as to sequence. The majority on the sequence homology with West Nile Virus was in the terminal loop (78%). The 40 nt 3p arm demonstrated 60% homology, decreasing at the distal segment. The 5p arm demonstrates on 42% sequence homology.

ZIKV miRNA Candidates in MiRBase

The predicted miRNA sequence from ZIKV obtained from the secondary structure analysis (5'-UGGGAAAGACCAGAGAC UCCAUGAGUUUCCACCACGCUGGCCGCCAGGCA CAGAUCGCCGAACUUCGGCGGCCGGUGUGGGG AAAUCCAUGGUUUCU-3') was studied using MiRBase in search of human hsa--mir homologues. The 5' end was extended 7 nt ~~in order~~ to include the flanking sequence that included the nearest UG motif.

An 84 single stem loop sequence corresponding to hsa-mir-147a (accession number MI0000262) + strand (E-value 7.0) was obtained in the 3' terminal loop extending into the 3p 56-90 arm. The overall sequence homology was greatest in the 3p arm (5'-GGCCGGUGUGGGGAAAUCCAUGGUUUCU-3') and not in the terminal loop (5'-CGCCGAACUUCGGC-3').

ZIKV|3'UTR|gi|226377833/1-54
CCAGGCACAGAUCGCCGAACUUCGGCGGCCGGU GUGGGGAAAUCCAUGGUUUCU--hsa-mir-147a|mat ure/1-20
----------GUGUGUGGAAAUGC-----UU CUGC

Hsa-mir-147 is a member of gene family MIPF0000105, mir-147. The mature sequence is 5'-GUGUGUGGAAAUGCUUCUGC-3' corresponding to the region of homology with 3p arm of the ZIKV stem loop, position 75-90, upstream from the essential GUG motif mismatch (Figure 10).

Figure 10. Mir-147 mature miRNA (MIMAT0000251) secondary structure.

The stem loop sequence of the validated hsa-mir-147 was visualized with Mfold. The mature hsa-mir-miRNA sequence, 5'-GUGUGGGGAAAUCCAU-3' and hybridizes to the 3' UTR target sequence, CCACACA, is highlighted in green.

TARGETS

There are 251 predicted targets for hsa-miR-147a in miRDB (*See Supplemental Files*). **Table 4** lists those targets with a score greater than 90. Neurofascin, rank number 7, functions include cell adhesion, ankyrin-binding protein which may be involved in neurite extension, axonal guidance, synaptogenesis, myelination and neuron-glial cell interactions. Most importantly, anti-neurofascin autoantibodies have been reported in Guillan-Barre Syndrome.

Table 4. miRDB Targets of hsa-mir-147a

Target Rank	Target Score	miRNA Name	Gene Symbol	Gene Description
1	99	hsa-miR-147a	BMP4	bone morphogenetic protein 4
2	98	hsa-miR-147a	CREBRF	CREB3 regulatory factor
3	98	hsa-miR-147a	KIAA1549L	KIAA1549-like
4	98	hsa-miR-147a	ACLY	ATP citrate lyase
5	98	hsa-miR-147a	C2orf61	chromosome 2 open reading frame 61
6	97	hsa-miR-147a	BCOR	BCL6 corepressor
7	96	hsa-miR-147a	NFASC	Neurofascin
8	96	hsa-miR-147a	PCMT1	protein-L-isoaspartate (D-aspartate) O-methyltransferase
9	96	hsa-miR-147a	PDE4D	phosphodiesterase 4D, cAMP-specific
10	95	hsa-miR-147a	CYP2S1	cytochrome P450, family 2, subfamily S, polypeptide 1
11	94	hsa-miR-147a	IGLON5	IgLON family member 5
12	93	hsa-miR-147a	SV2A	synaptic vesicle glycoprotein 2A
13	93	hsa-miR-147a	HDLBP	high density lipoprotein binding protein
14	92	hsa-miR-147a	ZEB2	zinc finger E-box binding homeobox 2
15	92	hsa-miR-147a	C11orf87	chromosome 11 open reading frame 87
16	92	hsa-miR-147a	NR3C1	nuclear receptor subfamily 3, group C, member 1 (glucocorticoid receptor)
17	91	hsa-miR-147a	NF1	neurofibromin 1
18	91	hsa-miR-147a	PLXNA2	plexin A2
19	91	hsa-miR-147a	DCLK3	doublecortin-like kinase 3

Three of these (BMP4, NF1, and ZEB2) were found to be involved in telencephalon development (GO:0021537) using DAVID (Huang et al., 2009a; Huang et al., 2009b) Telencephalon development is the paired anteriolateral division of the prosencephalon and the lamina terminalis from which the olfactory lobes, cerebral cortex, and subcortical nuclei are derived. The same three proteins are also involved in forebrain development, including the cerebral hemispheres, the thalamus, the hypothalamus, and the sensory and associative information processing, visceral functions, and voluntary motor function control centers [42, 43, 44].

Hsa-mir-147a appears to target the CCACACA motif in the 3' UTR of neurofascin (seed location 5851-5857; 5937-5943). The mir-147a binding sequence, GGUGUGU, has significant homology to ZIKV 3p arm motif, GGUGUGG, suggesting a ZIKV miRNA could also bind in a similar fashion to repress the Neurofascin transcript.

>Neurofascin 3'UTR| NM_015090

5821 GACCCCGGAG GACCTCCTGC CCCGCCCCCA **CCACACA**CCC ATATCCCCCA CCATTCCAAT

5881 TTGTTCTTTC CCGTGGGGAA TTTTTTTTCC CAGCGTCTCC ATCCCTTCCT ACATAT**CCAC**

5941 **ACA**CACACAA ATTGGTCTGA TCTTTTTTCC ATTGGTTAAA CATTTAACTC CATGCCAGAC

ZIKV HYBRID with Neurofascin

To evaluate a hybrid with Neurofascin, a 4620 nt sequence of the 3' UTR including the CCACACA seed region was analyzed with a 21 nt sequence from the ZIKV 3' arm (5'-GGCCGGUGUGGGGAAAUCCAU-3'). A significant 9 mer predicted binding region was identified downstream from the original seed region, also an 8 mer match. Both seed regions were separated by a single nucleotide (Figure 11). This would effectively be predicted to be capable of repressing transcription of the NFASC gene and cause a Guillan-Barre Syndrome similar to the anti-neurofascin autoantibodies reported to cause GBS.

Figure 11. Predicted ZIKV-NAFSC Hybrid

The predicted ZIKV mature miRNA sequence was hybridized with the predicted 3' UTR sequence from Neurofascin and analyzed with RNAHybrid. The ZIKV sequence, 5'-GGCCGGUGUGGGGAAAUCCA-3', in 3p stem loop arm was found to have a significant hybrid match to the NFASCN 3' UTR, 5'-CUGGAUUUCCUCCAACACC-3'.

Discussion

The World Health Organization (WHO) has declared Causality Framework as a priority towards understanding the pathogenicity of Zika virus in lieu of the reported incidences of microcephaly and Guillan-Barre Syndrome. To answer this, we append our list to include a potential miRNA in the sfRNA of Zika virus.

As of this report, only one miRNA has been reported in Flaviviridae, the closely related West Nile Virus. The Vir-MiR database has 171 potential candidates, but none for ZIKV. The ZIKV sfRNA 3' UTR that appears to contain a miRNA at the 3' end needs conclusive laboratory evidence of its existence in that the

neurofascin target could very well be responsible for the reported incidence on GBS in adults infected with Zika virus, and microcephaly due to gestational Zika virus infection.

The Neurofascin (NFASC) gene encodes three glial and neuronal isoforms of neurofascin (NFASC-140, NFASC-155, and NFASC-186) with key functions in assembling the nodal macromolecular complex, cell adhesion, ankyrin-binding protein (which may be involved in neurite extension), axonal guidance, synaptogenesis, myelination and neuron-glial cell interactions . NFASC-140 is a neuronal protein strongly expressed during mouse embryonic development. Expression of NFASC-140 persists but declines during the initial stages of node formation, in contrast to NFASC-155 and NFASC-186, which increase. Nevertheless, NFASC-140 can cluster voltage-gated sodium channels (Nav) at the developing node of Ranvier and can restore electrophysiological function independently of NFASC-155 and NFASC-186. This suggests that NFASC-140 complements the function of Nfasc155 and Nfasc186 in initial stages of the assembly and stabilization of the nodal complex. NFASC-140 is reexpressed in demyelinated white matter lesions of postmortem brain tissue from human subjects with multiple sclerosis. This expands the critical role of the NFASC gene in the function of myelinated axons and reveals further redundancy in the mechanisms required for the formation of this crucial structure in the vertebrate nervous system. [24].

Anti-neurofascin autoantibodies have been reported in Guillan-Barre Syndrome, combined central and peripheral demyelination disease (CCPD), Multiple Sclerosis (MS), and encephalitis [25-29]. As such, a virus-encoded miRNA from ZIKV with significant homology to hsa-mir-147 that is known to target neurofascin, is a compelling concept and worthy of further investigation. Guillain–Barré Syndrome is a transient, post-infectious disorder with onset at ~10 days and normally resolves within 30 days, it would be imperative to consider how a miRNA from Zika virus might contribute in the pathogenicity. The highly conserved secondary structures within the subgenomic Flavivirus RNA (sfRNA) of the 3' UTR were resistant to host nucleases and responsible for the observed cytopathology and pathogenicity. A contained, functioning Zika virus miRNA therefore could result in emergence of GBS if appropriate therapy is not directed towards that segment and may not respond to conventional immune therapies.

The next phase of research should initially validate this Zika virus encoded-miRNA, similar to the West Nile Virus, and validate all identified targets (neurofascin, synaptic vesicle glycoprotein 2A, neurofibromin 1, SAM and SH3 domain containing 1, neurogenin 2, others) that have been identified in the course of this study. The same miRNA-like small RNA in a 3' untranslated region is found in West Nile virus and has been shown to up-regulate GATA4 expression. GATA4, a zinc finger transcription factor, has been shown to be expressed during neural crest formation .GATA4 resides in 8p23; a 8p23 deletion syndrome is known as a malformation syndrome with clinical symptoms of facial anomalies, microcephaly, mental retardation, and congenital heart defects (CHD), however CNV variation in GATA4 appears unrelated to CHD (Guida et al., 2010 [41]). MCPH1 is also nearby (Bhatia et al., 1999), and co-localized genes are often co-regulated. We have elsewhere explored the plausibility of MCPH1 involvement in p53-BAX mediated apoptosis [37]. GATA4 also regulates Nf-kB and has been shown in excess to move cells into a phase of senescence (Kang et al., 2015 [38]).Additional co-factors remain unexplored and should be included in epidemiological studies (Lyons-Weiler et al., in review [37]).Additionally, mutations in either the mature miRNA segment or host target genes may exist that make binding more likely in some individuals and should be examined as a potential co-factor.

The risk of microcephaly due to Zika infection has been reported to be to 1% at this time (Cao-Lormeau et al., 2016)[45]. Our study has lessons for future studies of the etiology and mechanisms of pathologies of viruses, including Zika; miRNAs can have multiple divergent and convergent effects on genome regulation. We propose that miRNA-targeted treatments may be therefore considered keystone treatments that may be more effective than treatments that target individual proteins. Treatments aimed at silencing this Zika virus encoded-miRNA may be effective in the prevention of Flavivirus-induced pathologies.

References

1. Chambers TJ, Hahn CS, Galler R, Rice CM. Flavivirus genome organization, expression, and replication. Annu Rev Microbiol. 1990;44:649-88. Review. PubMed PMID: 2174669.
2. Pijlman GP, Funk A, Kondratieva N, Leung J, Torres S, van der Aa L, Liu WJ, Palmenberg AC, Shi PY, Hall RA, Khromykh AA. A highly structured,nuclease-resistant, noncoding RNA produced by flaviviruses is required for pathogenicity. Cell Host Microbe. 2008 Dec

11;4(6):579-91. doi: 10.1016/j.chom.2008.10.007. PubMed PMID: 19064258.
3. Lagos-Quintana M, Rauhut R, Lendeckel W, Tuschl T (2001) Identification of novel genes coding for small expressed RNAs. Science 294: 853–85 doi:.1126/science.1064921
4. Lau NC, Lim LP, Weinstein EG, Bartel DP (2001) An abundant class of tiny RNAs with probable regulatory roles in caenorhabditis elegans. Science 294: 858–862. doi: 10.1126/science.1065062
5. Lee RC, Ambros V (2001) An extensive class of small RNAs in caenorhabditis elegans. Science 294: 862–864. doi: 10.1126/science.1065329
6. Denli AM, Tops BB, Plasterk RH, Ketting RF, Hannon GJ. Processing of primary microRNAs by the Microprocessor complex. Nature. 2004 Nov 11;432(7014):231-5. Epub 2004 Nov 7. PubMed PMID: 15531879.
7. Gregory RI, Yan KP, Amuthan G, Chendrimada T, Doratotaj B, Cooch N, Shiekhattar R. The Microprocessor complex mediates the genesis of microRNAs. Nature. 2004 Nov 11;432(7014):235-40. Epub 2004 Nov 7. PubMed PMID: 15531877.
8. Landthaler M, Gaidatzis D, Rothballer A, et al. Molecular characterization of human Argonaute-containing ribonucleoprotein complexes and their bound target mRNAs. RNA. 2008;14(12):2580-2596. doi:10.1261/rna.1351608.
9. Han J, Lee Y, Yeom KH, Nam JW, Heo I, Rhee JK, Sohn SY, Cho Y, Zhang BT, Kim VN. Molecular basis for the recognition of primary microRNAs by the Drosha-DGCR8 complex. Cell. 2006 Jun 2;125(5):887-901. PubMed PMID: 16751099.
10. Auyeung, Vincent C. Beyond Secondary Structure: Primary-Sequence Determinants License Pri-miRNA Hairpins for Processing. Cell , Volume 152 , Issue 4 , 844 - 858
11. Fang W, Bartel DP. The Menu of Features that Define Primary MicroRNAs and enable De Novo Design of MicroRNA Genes. Mol Cell. 2015 Oct 1;60(1):131-45. doi: 10.1016/j.molcel.2015.08.015. Epub 2015 Sep 24. PubMed PMID: 26412306; PubMedCentral PMCID: PMC4613790
12. Nguyen TA, Jo MH, Choi YG, Park J, Kwon SC, Hohng S, Kim VN, Woo JS. Functional Anatomy of the Human Microprocessor. Cell. 2015 Jun 4;161(6):1374-87. doi: 10.1016/j.cell.2015.05.010. Epub 2015 May 28. PubMed PMID: 26027739.
13. R Ricketson, SM Christensen. Computational Evidence For A Viral Encoded Mirna In The Intergenic, Untranslated Region Of The Zaire Ebolavirus Nucleoprotein Gene May Explain Its Differential Virulence: A Potential Pandora Element. WebMedCentralPlus, March 15, 2015, Article ID: WMCPLS00512; ISSN 2051-0799]
14. RP Kincaid, CS Sullivan. Virus-Encoded microRNAs: An Overview and a Look to the Future. PLOS Pathogens, December 20, 2012. DOI: 10.1371/journal.ppat.1003018
15. M. Zuker. Mfold web server for nucleic acid folding and hybridization prediction.. Nucleic Acids Res. 31 (13), 3406-15, (2003)
16. Gruber AR, Lorenz R, Bernhart SH, Neuböck R, Hofacker IL. The Vienna RNA Websuite. Nucleic Acids Res. 2008. Lorenz, R. and Bernhart, S.H. and Höner zu Siederdissen, C. and Tafer, H. and Flamm, C. and Stadler, P.F. and Hofacker, I.L. “ViennaRNA Package 2.0
17. RNAFold. Algorithms for Molecular Biology, 6:1 page(s): 26, 2011
18. Matthews Lab; . Reuter, J. S., & Mathews, D. H. (2010). RNAstructure: software for RNA secondary structure prediction and analysis. BMC Bioinformatics. 11,129.
19. Li S-C, Shiau C-K, Lin W. Vir-Mir db: prediction of viral microRNA candidate hairpins. Nucleic Acids Research. 2008;36(Database issue):D184-D189. Doi:10.1093/nar/gkm610
20. Waterhouse, A.M., Procter, J.B., Martin, D.M.A, Clamp, M. and Barton, G. J. (2009) “Jalview Version 2 – a multiple sequence alignment editor and analysis workbench” Bioinformatics25 (9) 1189-1191 doi: 10.1093/bioinformatics/btp033
21. RNAHybrid. http://bibiserv.techfak.uni-bielefeld.de/rnahybrid
22. Rehmsmeier M, Steffen P, Hochsmann M, Giegerich R. Fast and effective prediction of microRNA/target duplexes. RNA. 2004 Oct;10(10):1507-17. PubMed PMID: 15383676; PubMed Central PMCID: PMC1370637
23. VARNA. http://varna.lri.fr
24. Zhang, A; Desmazieres, A; Zonta, B; Melrose, S; Campbell, G; Mahad, D; Li, Q; Sherman, DL; Reynolds, R; Brophy, PJ, Ng, King Man (2012): Anti-neurofascin antibodies: assay development and analysis of inflammatory diseases in the peripheral and central nervous system. Dissertation, LMU München: Graduate School of Systemic Neurosciences (GSN)]
25. Willison H. Neurofascin as target of autoantibodies in Guillain–Barré syndrome. Brain May 2011, 134 (5) e174; DOI: 10.1093/brain/awq375
26. Kawamura N, Yamasaki R, Yonekawa T, Matsushita T, Kusunoki S, Nagayama S,Fukuda Y, Ogata H, Matsuse D, Murai H, Kira J. Anti-neurofascin antibody in patients with combined central and peripheral demyelination. Neurology. 2013 Aug 20;81(8):714-22. doi: 10.1212/WNL.0b013e3182a1aa9c. Epub 2013 Jul 24. PubMed PMID: 23884033.
27. Mathey EK, Derfuss T, Storch MK, Williams KR, Hales K, Woolley DR, Al-Hayani A, Davies SN, Rasband MN, Olsson T, Moldenhauer A, Velhin S, Hohlfeld R, Meinl E,
28. Linington C. Neurofascin as a novel target for autoantibody-mediated axonal injury. J Exp Med. 2007 Oct 1;204(10):2363-72. Epub 2007 Sep 10. PubMed PMID: 17846150; PubMed Central PMCID: PMC2118456.,
29. Lindner M, Ng JK, Hochmeister S, Meinl E, Linington C. Neurofascin 186 specific autoantibodies induce axonal injury and exacerbate disease severity in experimental autoimmune encephalomyelitis. Exp Neurol. 2013 Sep;247:259-66. doi: 10.1016/j.expneurol.2013.05.005. Epub 2013 May 18. PubMed PMID: 23688679
30. Kozomara A, Griffiths-Jones S. NAR 2014 42:D68-D73 miRBase: integrating microRNA annotation and deep-sequencing data.

31. Kozomara A, Griffiths-Jones S.NAR 2011 39:D152-D157miRBase: tools for microRNA genomics.
32. Griffiths-Jones S, Saini HK, van Dongen S, Enright AJ.NAR 2008 36:D154-D158miRBase: microRNA sequences, targets and gene nomenclature.
33. Griffiths-Jones S, Grocock RJ, van Dongen S, Bateman A, Enright AJ.NAR 2006 34:D140-D144The microRNA Registry. Griffiths-Jones S. NAR 2004 32:D109-D111
34. Ambros V, Bartel B, Bartel DP, Burge CB, Carrington JC, Chen X, Dreyfuss G, Eddy SR, Griffiths-Jones S, Marshall M, Matzke M, Ruvkun G, Tuschl T. A uniform system for microRNA annotation. RNA 2003 9(3):277-279
35. Meyers BC, Axtell MJ, Bartel B, Bartel DP, Baulcombe D, Bowman JL, Cao X, Carrington JC, Chen X, Green PJ, Griffiths-Jones S, Jacobsen SE, Mallory AC, Martienssen RA, Poethig RS, Qi Y, Vaucheret H, Voinnet O, Watanabe Y, Weigel D, Zhu JK. Criteria for annotation of plant MicroRNAs. Plant Cell. 2008 20(12):3186-3190
36. Hussain M, Torres S, Schnettler E, et al. West Nile virus encodes a microRNA-like small RNA in the 3 ′ untranslated region which up-regulates GATA4 mRNA and facilitates virus replication in mosquito cells. Nucleic Acids Research. 2012;40(5):2210-2223. doi:10.1093/nar/gkr848.
37. Lyons-Weiler, J., R. Ricketson, E.F. Fogarty and G. Macgregor-Skinner. in review. Areas of Research and Preliminary Evidence on Microcephaly, Guillain-Barré Syndrome and Zika Virus Infection in the Western Hemisphere. PLOS One, PONE-D-16-09495
38. Kang C et al., 2015. The DNA damage response induces inflammation and senescence by inhibiting autophagy of GATA4. Science. 2015 Sep 25;349(6255):aaa5612. doi: 10.1126/science.aaa5612.
39. Bhatia SN et al., 1999. Prenatal detection and mapping of a distal 8p deletion associated with congenital heart disease. Prenat Diagn. 19(9):863-7.
40. http://eriba.umcg.nl/wp-content/uploads/2016/01/Demaria-2015-09-25-Science.pdf
41. Guida V, Lepri F, Vijzelaar R, De Zorzi A, Versacci P, Digilio MC, Marino B, De Luca A, Dallapiccola B. 2010. Multiplex ligation-dependent probe amplification analysis of GATA4 gene copy number variations in patients with isolated congenital heart disease. Dis Markers. 28(5):287-92. doi: 10.3233/DMA-2010-0703.
42. Huang DW, Sherman BT, Lempicki RA. 2009a. Systematic and integrative analysis of large gene lists using DAVID Bioinformatics Resources. Nature Protoc. 4(1):44-57.
43. Huang DW, Sherman BT, Lempicki RA. 2009b. Bioinformatics enrichment tools: paths toward the comprehensive functional analysis of large gene lists. Nucleic Acids Res. 37(1):1-13.
44. Marin, O. and Rubenstein, JL. 2003. Cell migration in the forebrain. Annual Review of Neuroscience [2003, 26:441-483]
45. Cao-Lormeau VM, Blake A, Mons S, Lastère S, Roche C, Vanhomwegen J, Dub T, Baudouin L, Teissier A, Larre P, Vial AL, Decam C, Choumet V, Halstead SK, Willison HJ, Musset L, Manuguerra JC, Despres P, Fournier E, Mallet HP, Musso D, Fontanet A, Neil J, Ghawché F. 2016. Guillain-Barré Syndrome outbreak associated with Zika virus infection in French Polynesia: a case-control study. Lancet. pii: S0140-6736(16)00562-6. Doi: 10.1016/S0140-6736(16)00562-6.
46. Y. Byun and K. Han, PseudoViewer3: generating planar drawings of large-scale RNA structures with pseudoknots, Bioinformatics, Vol. 25, 1435-1437, 2009.
47. Y. Byun and K. Han, PseudoViewer: web application and web service for visualizing RNA pseudoknots and secondary structures, Nucleic Acids Research, Vol.34, W416-W422, 2006.
48. K. Han and Y. Byun, PseudoViewer2: visualization of RNA pseudoknots of any type, Nucleic Acids Research, Vol. 31, No. 13, 3432-3440, 2003.
49. K. Han, Y. Lee and W. Kim, PseudoViewer: Automatic Visualization of RNA Pseudoknots, Bioinformatics, Vol. 18, S321-S328, 2002.

Illustrations

Illustration 1

FIGURE 1. Features of a Canonical miRNA The 5’ flanking sequence contains a UG motif whereby the uracil is occasionally substituted by an adenine (A) with continued processing towards a mature miRNA. A GUG mismatch motif is located in the proximal stem loop structure duplex, and an apical (G)UG motif is identified in the 5p-terminal loop junction. The 3p arm usually terminates in a CNNC motif (not shown).

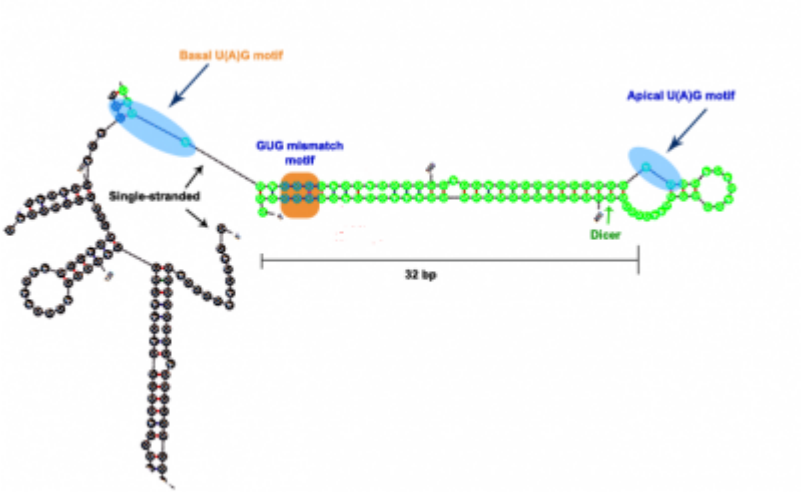

Illustration 2

Figure 2. Secondary structure of ebv-mir-BART1 The secondary structure of the validated Epstein - Barr virus miRNA, ebv-mir-BART1, was generated with Mfold [15]. The 5’ terminus contains a UG motif and a UGU mismatch region. The Terminal loop is 6 nt in length,, and the GUG motif is not predicted to be in the 5’ region of the terminal loop but in the downstream region of the 5’

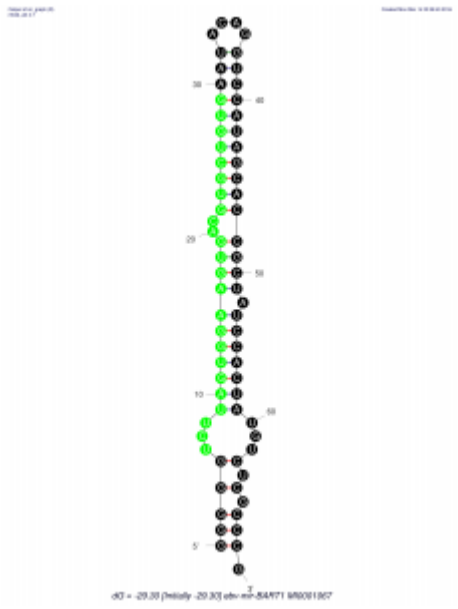

Illustration 3

Figure 3. The secondary structure of the Zika virus sfRNA of the 3' UTR (428 nt) was generated in Mfold using default parameters. The stem loop structure (MFE -167.68) from 343-428 is highlighted. Pseudoknots cannot be predicted in Mfold and predictions of peudoknots were obtained with RNAStructure and visualized with VARNA [23].